Phase composition and mechanical properties of Cu-Ti alloys synthesized in the surface layer of copper by plasma impact on the Ti/Cu system

N.N. Cherenda[1,2], A.V. Basalai[3], V.V. Uglov[1,2], A.P. Laskovnev[3], V.M. Astashynski[4], A.M. Kuzmitski[4]*

[1]Belarusian State University, Nezavisimosti ave., 4, Minsk 220030, Belarus

[2]National Research Tomsk Polytechnic University, Lenin ave., 2a, Tomsk 634028, Russia

[3]Physical Technical Institute of the National Academy of Sciences of Belarus, Kuprevicha str. 10, Minsk 220141, Belarus

[4]A.V. Luikov Heat and Mass Transfer Institute, National Academy of Sciences of Belarus, P. Brovki str., 15, Minsk 220072, Belarus

Abstract

Cu-Ti alloys synthesized in the surface layer of copper by means of preliminary Ti coating deposition and subsequent treatment by compression plasma flows have been investigated in this work. X-ray diffraction, scanning electron microscopy, energy-dispersion X-ray microanalysis, Auger electron spectroscopy, Vickers microhardness measurements and tribological tests were used for Cu-Ti alloys characterization. The findings showed that the increase of the energy absorbed by the surface layer during plasma treatment from 57 to 74 J/cm^2 per pulse resulted in the growth of the alloyed surface layer thickness from 15 to 19 μm, more homogeneous distribution of Ti in the alloyed layer and the decrease of Ti average concentration from 13.1 to 9.7 at.% in it. The supersaturated solid solution of titanium in copper is the main phase constituent of the alloyed layer after treatment at 74 J/cm^2. The synthesized surface of the Cu-Ti alloy possesses enhanced strength and tribological properties.

Key words: copper, titanium, compression plasma flow, phase and element composition, microhardness, friction coefficient.

Corresponding author: Tel. +375 17 209 55 90, E-mail cherenda@bsu.by

Introduction

Copper and copper alloys are widely used in industry mainly due to their high electrical and thermal conductivity [1]. Cu-Be alloys have a good combination of strength and electrical conductivity providing commercial application of this group of alloys. At the same time the usage of toxic beryllium and high production costs are the main disadvantages of Cu-Be alloys [2]. Nowadays Cu-Ti alloys are considered as a substitution of beryllium containing alloys [2-5]. These alloys possess high mechanical properties and relatively high electrical conductivity though it is less than that for Cu-Be alloys [2-9].

The concentration of titanium in Cu-Ti alloys usually varies in the range of 1-6 at.%. The maximum titanium concentration in the alloy corresponds to the maximum solubility limit of titanium in the copper solid solution on the equilibrium Cu-Ti phase diagram [3]. Thus, the structure of a Cu-Ti alloys providing desired mechanical properties is formed during ageing and mainly consists of Cu(Ti) solid solution and α-Cu_4Ti or β-Cu_4Ti intermetallides [4]. The presence of titanium in a copper solid solution makes worse electrical conductivity though it can be increased by ageing in hydrogen containing atmosphere [2, 10, 11]. Mechanical properties, e.g. hardness and wear resistance, of Cu-Ti alloys surface layers can be improved by different surface treatment techniques: ion implantation [12], plasma nitriding [13] and plasma carburization [14].

Surface treatment techniques can also be applied for the formation of Cu-Ti alloys in the copper surface layer [15-17]. This approach is very prospective when enhancement of copper surface properties mainly is required e.g. the increase of copper sliding contacts wear resistance. In particular, in [15, 16] it was reported on the formation of Cu-Ti surface alloys containing 4-87 wt.% Ti using the double glow discharge process. The thickness of the alloyed layers was up to 120 μm and their phase composition was the mixture of Cu(Ti), CuTi and Cu_4Ti. The synthesized alloys had high hardness (up to 7 GPa) and high wear resistance. Laser treatment of the Ti coating (the thickness of 0.15 mm)/ Cu system resulted in the formation of the alloyed with titanium layer with the thickness of ~ 1 mm containing 25-85 wt.% Ti [17]. The formation of equilibrium intermetallides with different stoichiometry (Cu_4Ti, Cu_2Ti, $CuTi_2$, Cu_4Ti_3) led to the hardness increase up to 7 GPa.

Compression plasma flows (CPF) generated by quasi-stationary plasma accelerators can also be used for synthesis of the surface alloys [18, 19]. Such plasma flows with comparatively long life-time (~100 μs) are characterized by the presence of a compression area in the middle of a plasma flow that appears due to the interaction of a longitudinal component of the discharge current 'swept away' from the discharge device with the intrinsic azimuth magnetic field [20]. CPF possess a high temperature (1-3 eV) and a high velocity ((4-7)·10^6 cm/s) of plasma particles

resulting in high density of energy absorbed by the surface of the treated material (up to ~10^2 J/cm^2). The length of the plasma flow is about 10 - 12 cm. In the zone of the maximum contraction it constitutes 1 cm in diameter. The details of the plasma accelerator construction and principles of plasma flows generation are described in [20]. Surface layer alloying includes preliminary deposition of the coating containing one or more alloying elements and subsequent treatment by CPF. A similar approach was used for the synthesis of Cu-Cr alloys at the copper surface by successive operations of Cr film deposition and subsequent treatment with a low-energy high-current electron beam [21]. For surface layer alloying CPF treatment regimes should provide melting of both the coating and the surface layer of the substrate. Therefore, the thickness of the melt must be greater than that of the coating. Mixing of the coating and substrate elements in the melt occurs due convection processes initiated by hydrodynamic instabilities in the plasma-melt system [19, 20, 22, 23]. Subsequent crystallization takes place in conditions of high-speed cooling resulting in grains refinement and metastable phases formation [18, 19]. At this stage additional phases formation at the surface of the alloyed layer occurs due to the interaction of residual chamber gases with the surface. In particular, δTiN formation in the surface layer with the thickness of ~ 70 nm was found after alloying the steel by Ti atoms while using nitrogen as a plasma forming gas [18]. The concentration of the coating element in the alloyed layer depends on the coating thickness and CPF treatment regimes (the energy absorbed by the surface layer and the number of pulses). The increase of both energy absorbed by the surface layer and the number of pulses leads to the alloying element concentration decrease. This dependence is explained by redistribution of the coating element in the melt with the greater thickness. Another reason of this effect is the growth of the surface erosion intensity. Erosion of the surface layer during plasma impact diminishes the volume of the alloying element that can be redistributed in the melt by convection processes. Hydrodynamic flow of the melt from the center of the sample to its edge caused by plasma movement along the surface is the main reason for erosion [24, 25].

It was already shown [20, 21] that alloying of plain carbon steels by different elements under CPF treatment resulted in the formation of the alloyed layer with the thickness of tens of micrometers and enhanced mechanical properties, thus allowing one to consider that this approach is potentially interesting for industrial applications. At the same time CPF treatment drawbacks such as the formation of developed surface waviness and a comparatively small treatment area (10-12 cm^2) should be taken into account.

The synthesis of Cu-Ti alloys with a different concentration of Ti in the copper surface layer by means of Ti/Cu treatment by CPF and the investigation of their phase and elemental composition, mechanical properties were the main aims of this work.

Experimental

The samples of a pure copper (the concentration of impurities was not greater than 0.08 wt.%) were investigated. The samples size was 10x15 mm and the thickness - 3 mm. The samples were cut from a rolled copper plate. The titanium coating was deposited on copper samples by means of vacuum arc deposition. The thickness of the coatings was 3 μm. The samples of the copper and samples of the Ti/Cu system were treated by compression plasma flows generated in the magneto-plasma compressor of compact geometry [20]. Nitrogen was used as a plasma forming gas. Nitrogen pressure in the vacuum chamber was 400 Pa before each pulse. The samples of Ti/Cu system were placed in the vacuum chamber at the distance of 8, 10 and 12 cm from the electrodes which corresponded to the energy density of heat flux absorbed by the sample (Q) of 74, 68 and 57 J/cm^2 per pulse, respectively (registered by calorimetric measurements). Energy density was varied with aim of copper alloys synthesis with different concentration of titanium. Treatment was carried out by three pulses at the interval of ~ 5 s.

The phase composition of the copper alloyed layers was investigated by means of X-ray diffraction (XRD) with the Ultima IV RIGAKU diffractometer in Cu Kα radiation. The analysis of cross-section morphology was carried out by means of scanning-electron microscopy (SEM) using the LEO 1455 VP microscope. Before SEM investigations the samples cross-section was etched in $FeCl_3$–HCl–C_2H_5OH solution. The element composition analysis was carried out by energy dispersion X-ray microanalysis (EDX) using the Oxford X-ray detector and by means of Auger electron spectroscopy (AES) using the PHI-660 spectrometer combined with sputtering by Ar ions. Ti concentration was determined by EDX at the surface of the samples (X-ray generation depth ~ 1 μm) using the smallest magnification of SEM view to avoid influence of Ti distribution local inhomogeneity on the determined concentration value. The microhardness was measured using the MVD 402 Wilson Instruments equipment (Vickers diamond indentor). The maximum indentation depth was estimated as d/7, where d is the average size of the indentation diagonal. Preliminary measurements of microhardness were carried out at the loads of 0.25, 0.5 and 1.0 N. At the same time measurements with the load less than 1 N result in a very high error because of surface waviness after CPF treatment. Therefore, the results of the microhardness measurements at the load of 1.0 N only are given in this work. The tribological test was made on the pin-on-plane type tribometer under conditions of dry sliding friction and the load of 0.5 N. The linear velocity of the pin (92 wt.% WC, 8 wt.% Co) was 0.4 cm/s.

Results and discussion

Copper possesses a high value of thermal conductivity that is why for copper alloying it was necessary to determine CPF critical treatment regime that provides melting of the surface layer. Numerical solution of the one-dimensional heat conduction equation was made to estimate the minimal value of the energy absorbed by the surface layer sufficient for surface layer melting. Estimated value of the energy density is 35 J/cm^2. After that pure copper samples were treated by CPF in the range of density of energy absorbed by the surface layer 20 – 68 J/cm^2. Local areas of melting were found at the surface after treatment at 33 J/cm^2. CPF treatment at 57 J/cm^2 led to the formation of the melted layer with the thickness of 20 μm (Fig. 1). This value of Q was chosen as the minimal energy density for Ti/Cu system samples treatment to be sure that the melt life-time would be enough for initiation and development of convective mixing in the melt.

CPF impact on the samples of the Ti/Cu system at the energy absorbed by the surface layer in the range of 57-74 J/cm^2 resulted in the formation of the copper surface layer alloyed by titanium atoms. Cross-section images and distributions of characteristic Ti $K\alpha_1$ radiation along the depth of the Ti/Cu system samples after CPF treatment are presented in Fig. 2. One can see that the increase of energy absorbed by the surface layer leads to more homogeneous distribution of titanium in the alloyed layer. Formation of the local areas with a different Ti concentration is observed after CPF impact at Q=57 J/cm^2 (Fig. 2a, b) in spite of treatment with three plasma pulses. A great difference of the alloyed layer components melting temperature (T_{Ti}=1608 °C, T_{Cu}=1083 °C [26]) can be the cause of Ti inhomogeneous distribution. Such a difference leads to the reduction of the life-time of these elements liquid phases simultaneous existence during plasma impact and, hence, to diminishing duration of convective flows that are responsible for mixing in the melt. Uniform titanium distribution was found after CPF treatment at Q=74 J/cm^2 due to the increase of the surface layer temperature during impact and growth of the convection flows life-time (Fig. 2 c, d). The increase of the energy absorbed by the surface also leads to the rise of the alloyed layer average thickness from 15 μm (57 J/cm^2) to 19 μm (74 J/cm^2), diminishing Ti concentration in the alloyed layer due to titanium atoms redistribution in the melt with greater thickness (Fig. 3).

To investigate the possibility of the vacuum chamber residual atmosphere atoms presence in the surface layer Auger spectroscopy was used. The results of AES analysis are presented in Fig. 4. The findings showed the presence of nitrogen and oxygen peaks at the surface for both treatment regimes. The nitrogen content was greater than that of oxygen in the analyzed layer due to the fact that it was used as a plasma forming gas. Titanium distribution also has a peak at the surface. Both AES data and EDX data showed the decrease of Ti concentration in the depth of the alloyed layer with the growth of the energy absorbed by the surface. Similar distributions of nitrogen and titanium were observed by the non-Rutherford backscattering analysis after CPF

treatment of the Ti/steel system in [18] and were explained by δTiN formation, which was confirmed by XRD investigations. In conditions of these experiments the formation of phases from Ti-N-O and Cu-O systems can be supposed based on the AES data. The approximate thickness of the layer containing the increased concentration of N, O and Ti was ~ 0.1 μm, which was evaluated assuming that Cu sputtering rate was constant during AES measurements. This value correlates with the thickness of the nitrogen containing layer in the steel alloyed by Ti atoms under CPF impact [18].

EDX analysis showed that Ti concentration in the copper alloyed layer varied in the range of 9.7 – 13.1 at. % depending on the energy absorbed by the surface layer (Fig. 3). Similar values of Ti concentration (in the depth of the alloyed layer) were received by AES analysis (Fig. 4). The solubility limit of Ti in the copper solid solution does not exceed 8 at.% according to the equilibrium phase diagram [3, 27] though the solubility limit of 10 at.% at the temperature of eutectic transformation (870 °C) in equilibrium conditions can be found in literature [28]. Ti solubility limit decreases with the temperature diminishing. According to Ref. [29] it amounts to 1.5 at.% at 300 °C. Thus, one could expect the formation of Cu_4Ti intermetallides in the alloyed layer after CPF treatment. At the same time diffraction lines of Cu_4Ti were not found in the diffraction patterns of the treated samples (Fig. 5), which can be explained by the formation of tiny intermetallides that cannot be resolved during XRD investigations. A similar problem concerning XRD detection of Cu_4Ti phase was reported in [3]. The formation of the Cu(Ti) supersaturated substitution solid solution (later designated as Cu`(Ti)) in conditions of high speed cooling can be another cause of this effect. Ti concentration in the supersaturated solid solution can reach up to 10 at. % (the maximum value of Ti solubility limit [28]). At the same time it should be noted that the solubility limit depends on the cooling speed and may exceed approximate value of 10 at. %. Thus, most or all titanium atoms can be embedded in Cu crystalline lattice after CPF treatment.

The supersaturated solid solution formation is well seen on the diffraction patterns presented in Fig. 6. After CPF treatment at Q=57 J/cm^2 the diffraction lines at 2Θ angle position of ~ 74^o and ~ 90^o are the superposition of Cu and Cu`(Ti) diffraction lines. Incorporation of Ti atoms in Cu crystalline lattice results in the increase of the lattice parameter and the shift of solid solution diffraction lines to the area of lower angles (Fig. 6). Thus, at this treatment regime the phase composition of the analyzed layer consists of the mixture of Cu (or equilibrium Cu(Ti) solid solution) and Cu`(Ti) supersaturated solid solution. The calculated depth of X-ray penetration is about 8 μm (for the angle position of Cu (311) diffraction line), assuming that 75% of radiation is absorbed in the analyzed layer containing 10 at.% of Ti atoms. It means that the results of the phase composition analysis were obtained from the alloyed layer only, which is consistent with

the cross-section investigations by SEM (Fig. 2a and 2b) where mixture of alloyed and unalloyed copper areas is seen in the remelted layer. The increase of the energy absorbed by the surface layer leads to diminishing Ti concentration in the supersaturated solid solution (Fig. 3) and hence to diminishing Cu`(Ti) lattice parameter (Fig. 7) resulting in the shift of Cu`(Ti) diffraction lines toward positions of Cu standard diffraction lines. After treatment at 68 J/cm^2 overlapping of Cu and Cu`(Ti) diffraction lines is still seen on the diffraction pattern (Fig. 6). This overlapping disappears after treatment at 74 J/cm$^2$ (Fig. 6). The diffraction pattern at this treatment regime consists of diffraction lines of mainly one phase that can be assigned to Cu`(Ti). This is consistent with the data of SEM investigations where homogeneous distribution of Ti was found along the depth of alloyed layer (Fig. 2d).

It was also found that CPF treatment resulted in the copper solid solution texture formation. The texture coefficients (TC_{hkl}) for hkl diffraction planes calculated using the Harris method [30] are presented in Table. As the copper samples are made of a deformated copper plate the maximum TC is observed for (110) crystallographic planes. This texture became weaker after Ti coating deposition possibly due to recrystallization processes. After CPF treatment copper solid solution grains started to grow in <100> direction. This direction becomes preferential after treatment at Q=74 J/cm^2 (Table). The formation of columnar-like grains in the alloyed layer oriented almost perpendicularly to the surface is already seen in Fig. 1 and 2c. Direction <100> of the grains preferential growth in conditions of high speed cooling is typical of materials with a face-centered cubic lattice [31]. <100> direction provides the maximum growth speed of the crystal when it is close to the direction of heat sink during high speed cooling [31].

It should be noted that no diffraction lines of TiN or TiO_2 were found in the diffraction patterns in spite of the AES data and in contrast to the results on alloying of steel with Ti atoms obtained earlier [18].

Alloying of the copper surface layer by Ti atoms resulted in its microhardness increase (Fig. 8). The microhardness value after treatment varied in the range of 1.2-1.4 GPa depending on the treatment regimes. The microhardness of 2.5 GPa [6] and 1.4 GPa [9] were reported for bulk Cu-4 wt.% Ti alloy after quenching. According to the data presented in [9] for quenched Cu-10 at.% Ti alloy microhardness of 1.8 - 2 GPa should be expected, assuming that hardening only occurs due to solid solution hardening. Thus, the microhardness of Cu-Ti alloy received in this experiment seems to be less than microhardness reported in literature. At the same time the indenter penetration depth during microhardness testing was about 5-5.5 μm, which is 20-30% of the alloyed layer thickness. It is known that for accurate determination of the thin layer material microhardness the ratio of the indenter penetration depth and the film thickness should be at least 1:10 to avoid the influence of the substrate material [32]. Thus, in conditions of these

experiments the influence of a softer copper substrate on the measured microhardness can take place. The same reason can be used for the explanation of the microhardness growth with Q increase (Fig. 8) in spite of the Ti concentration decrease and fading influence of solid solution hardening. The growth of the alloying layer thickness and the formation of a uniform structure consisting of Cu`(Ti) only can be more crucial factors than the alloying concentration decrease. It should be noted that grains refinement (that is well seen on diffraction patterns (Fig. 6) due to diffraction lines broadening) can also influence on microhardness though this effect was not investigated in the work.

Alloying also resulted in diminishing the friction coefficient (Fig. 9). After CPF treatment the friction coefficient is about 0.1 (at the sliding distance of 8 m) that is 2.5 times less than that of the initial copper sample. Surface hardening is one of the causes of the friction coefficient decrease. Another cause is the formation of a wavy surface that is characteristic for metal surfaces melted under treatment by high-intensity plasma flows. It is seen from Fig. 10 that the wear track in the CPF treated sample is discontinuous. It consists of separate areas formed by the indenter sliding on the top of the surface waves. As a result, the contact area between the indenter and the surface diminishes, leading to the friction force and friction coefficient decrease. One can also notice that the width of the wear track in the treated sample is smaller than in the initial one under the same friction conditions, indicating the wear resistance increase (Fig. 10).

Conclusions

Compression plasma flows impact (3 pulses) on the samples of the Ti coating (3 μm thickness)/Cu system at the energy absorbed by the surface layer in the range of 57-74 J/cm^2 per pulse resulted in the formation of the copper surface layer alloyed by titanium atoms. The increase of the energy absorbed by the surface led to the rise of the alloyed layer average thickness from 15 μm to 19 μm causing Ti concentration diminishing in the alloyed layer from 13.1 to 9.7 at. %. Surface segregation of titanium was found due to the interaction between the surface atoms and the residual gases of the vacuum chamber.

The growth of the energy absorbed by the surface also led to more homogeneous titanium distribution influencing the phase composition of the alloyed layer. After CPF treatment at Q=57 J/cm^2 per pulse the alloyed layer consisted of the copper and supersaturated solution of titanium in copper Cu`(Ti). Cu`(Ti) became the main constituent of the alloyed layer after CPF treatment at 74 J/cm^2 per pulse. The increase of the energy absorbed by the surface layer led to diminishing Cu`(Ti) lattice parameter due to the decrease of Ti concentration in the supersaturated solid solution. The formation of columnar-like grains of Cu`(Ti) in the alloyed layer grown in <100> direction was found after treatment at 74 J/cm^2 per pulse

Alloying of the copper surface layer by Ti atoms resulted in its microhardenss increase and friction coefficient decrease. The microhardness value after treatment varied in the range of 1.2-1.4 GPa depending on the treatment regimes. After CPF treatment the friction coefficient was about 0.1 (at the sliding distance of 8 m) that is 2.5 times less than that of the initial copper sample. Surface hardening is one of the causes of the friction coefficient decrease. Another reason is the formation of a wavy surface, which causes the decrease of the contact area between indenter and the surface.

Acknowledgements

The experimental investigations were partially carried out at Tomsk Polytechnic University within the framework of Tomsk Polytechnic University Competitiveness Enhancement Program grant.

References

1. H. Lipovsky, E. Arpaci, Copper in the automotive industry, VCH Verlag GmbH & Co., Weinheim, 2007.

2. S. Semboshi, T. Al-Kassab, R. Gemma, R. Kirchheim, Microstructural evolution of Cu-1 at% Ti alloy aged in a hydrogen atmosphere and its relation with the electrical conductivity, Ultramicroscopy 109(5) (2009) 593–598.

3. S. Semboshi, M. Ishikuro, S. Sato, K. Wagatsuma, T. Takasugi, Extraction of precipitates from age-hardenable Cu-Ti alloys, Materials Characterization, 82 (2013) 23–31.

4. Y. D. Zhu, M. F. Yan, Y. X. Zhang, C. S. Zhang, First-principles investigation of structural, mechanical and electronic properties for Cu–Ti intermetallics, Computational Materials Science 123 (2016) 70–78.

5. W. A. Soffa, D. E. Laughlin, High-strength age hardening copper-titanium alloys: Redivivus, Progress in Materials Science 49(3–4) (2004) 347–366.

6. F. Hernandez-Santiago, N. Cayetano-Castro, V. M. Lopez-Hirata, H. J. Dorantes-Rosales, J. D. J. Cruz-Rivera, Precipitation Kinetics in a Cu-4 mass % Ti Alloy.Materials Transactions 45(7) (2004) 2312–2315.

7. I. S. Batra, G. K. Dey, U. D. Kulkarni, S. Banerjee, On the sequence of clustering and ordering in a meltspun Cu-Ti alloy, Materials Science and Engineering A, 360(1–2) (2003) 220–227.

8. S. Nagarjuna, M. Srinivas, K. Balasubramanian, D. S. Sarma, The alloy content and grain size dependence of flow stress in Cu-Ti alloys, Acta Materialia 44(6) (1996) 2285–2293.

9. S. Nagarjuna, D. S. Sarma, On the variation of lattice parameter of Cu solid solution with solute content in Cu-Ti alloys, Scripta Materialia 41(4) (1999) 359–363.

10. S. Semboshi, T. Nishida, H. Numakura, Microstructure and mechanical properties of Cu-3 at.% Ti alloy aged in a hydrogen atmosphere, Materials Science and Engineering A 517(1–2) (2009) 105–113.

11. S. Semboshi, T. Takasugi, Fabrication of high-strength and high-conductivity Cu-Ti alloy wire by aging in a hydrogen atmosphere, Journal of Alloys and Compounds 580 (2013) S397-S400.

12. D. Ueyama, S. Semboshi, Y. Saitoh, F. Hori, K. Nishida, N. Soneda, A. Iwase, Modification of microstructure and hardness for Cu-Ti alloy by means of energetic ion beam irradiation, Nuclear Instruments and Methods in Physics Research, Section B: Beam Interactions with Materials and Atoms 341 (2014) 53–57.

13. S. Semboshi, S. Kimura, A. Iwase, N. Ohtsu, Surface hardening of age-hardenable Cu-Ti dilute alloys by plasma nitriding, Surface and Coatings Technology 258 (2014) 691–698.
14. S. Semboshi, A. Iwase, T. Takasugi, Surface hardening of age-hardenable Cu-Ti alloy by plasma carburization, Surface and Coatings Technology 283 (2015) 262–267.
15. Q. Yuan, C. Chi, Y. Su, Z. Xu, B. Tnag, Surface alloying of Cu with Ti double glow discharge process, Trans. Nonferrous Met. Soc. China 14(3) (2004) 516-519.
16. Y. Zhang, F. Chen, J. Lu, Y. Su, Z. Xu, Study of Titanizing the Surface of Copper Substrates by the Double Glow Discharge Plasma Surface Alloying Technique, Plasma Science and Technology 7(4) (2005) 2947-2949.
17. P. K. Wong, C. T. Kwok, H. C. Man, F. T. Cheng, Corrosion behavior of laser-alloyed copper with titanium fabricated by high power diode laser, Corrosion Science 57 (2012) 228–240.
18. N. N. Cherenda, V.V. Uglov, M.G. Poluyanova, V.M. Astashynski, A.M. Kuzmitski, A.D. Pogrebnjak, B. Stritzker, The influence of the coating thickness on the phase and element composition of a “Ti coating / steel” system surface layer treated by a compression plasma flow, Plasma Processes and Polymers 6 (2009) S178-S182.
19. V.V. Uglov, V.M. Anishchik, N.N. Cherenda, A.K. Stalmashonak, V.M. Astashinski, A.M. Kuzmickii, E.A. Kostyukevich, A.V. Kovyazo, Mixing of chromium/carbon steel by compressive plasma flows, Vacuum 78(2-4) (2005) 489-493.
20. V. V. Uglov, V. M. Anishchik, V. V. Astashynski, V. M. Astashynski, S. I. Ananin, V. V. Askerko, E. A. Kostyukevich, A. M. Kuz’mitski, N. T. Kvasov, A. L. Danilyuk, The effect of dense compression plasma flow on silicon surface morphology Surface and Coatings Technology 158–159 (2002) 273-276.
21. A. Markov, E. Yakovlev, D. Shepel, M. Bestett,. Synthesis of a Cr-Cu surface alloy using a low-energy high-current electron beam, Results in Physics 12 (2019) 1915-1924.
22. B. Bazylev, G. Janeschitz, I. Landman, S. Pestchanyi, A. Loarte, G. Federici, M. Merola, J. Linke, T. Hirai, A. Zhitlukhin, V. Podkovyrov, N. Klimov, Behaviour of melted tungsten plasma facing components under ITER-like transient heat loads. Simulations and experiments, Fusion Engineering and Design 83 (2008) 1077-1081.
23. A Ya Leyvi, A P Yalovets, Numerical study of mass transfer of a material under intense flows of high-speed electrons and plasma, IOP Conf. Series: Journal of Physics: Conf. Series 830 (2017) 012071-4.
24. V.I. Tereshin, I.E. Garkusha, A.N. Bandura, O.V. Byrka, V.V. Chebotarev, V.A. Makhlaj, D.G. Solyakov, H. Wuerz, Influence of plasma pressure gradient on melt layer macroscopic

erosion of metal targets in disruption simulation experiments, J. Nucl. Mater. 313–316 (2003) 685–689.
25. A.Ya. Leyvi, N.N. Cherenda, V.V. Uglov, A.P. Yalovets, The impact of a shock-compressed layer on the mass transfer of target material during processing compression plasma flows, Resource-Efficient Technologies 3 (2017) 222–225.
26. E.A. Brandes, G.B. Brook, Smithells Metals Reference Book, seventh edition, Butterworth Heinmann, Oxford, 1992.
27. M. A. Turchanin, P. G. Agraval and A. R. Abdulov, Thermodynamic Assessment of the Cu–Ti–Zr system. I. Cu−Ti system, Powder Metallurgy and Metal Ceramics 47(5-6) (2008) 344 - 360.
28. H. Okamoto, Cu-Ti (Copper-Titanium), Journal of Phase Equilibria, 26(3) (2002) 549-550.
29. Diagrammy sostoyaniya dvoinykh metallicheskikh sistem: spravochnik (Phase Diagrams of Binary Metal Systems: Handbook), Ed. N.P. Lyakishev, Vol 2, Mashinostroenie, Moscow, 1997. (in Russian)
30. G.B. Harris, Quantitative measurement of preferred orientation in rolled uranium bars, Phil. Mag. 43(336) (1952) 113-123.
31. Physical Metallurgy, Ed. R.W. Cahn and P.Haasen, Vol. 2. Elsevier Science B.V. 1996.
32. Alain Iost, Gildas Guillemot, Yann Rudermann, Maxence Bigerelle, A comparison of models for predicting the true hardness of thin films, Thin Solid Films 524 (2012) 229-237.

Table

Texture coefficients (TC_{hkl}) of hkl diffraction lines in patterns of initial sample Cu samples and samples of Ti/Cu system before and after CPF treatment

hkl plane	TC_{hkl}				
	Cu sample	Ti/Cu system sample	Ti/Cu system samples treated by CPF		
			57 J/cm^2	68 J/cm^2	74 J/cm^2
111	0,2	0,8	0,6	0,5	0,3
200	0,4	0,7	1,3	1,4	1,8
220	2,4	1,1	1,3	1,3	0,9
311	1,1	1,4	0,8	0,9	1,0

Figures caption

Fig. 1. Cross-section optical microscopy image of Cu sample treated by CPF at Q=57 J/cm^2.

Fig. 2. Cross-section SEM-images (a, c) and Ti distribution along the depth (b, d) of Ti/Cu samples treated by CPF at Q=57 J/cm^2 (a, b) and Q=74 J/cm^2 (c, d).

Fig. 3. Dependence of the Ti concentration (EDX data) in the surface layer of Ti/Cu system samples treated by CPF on the density of energy absorbed by the surface.

Fig. 4. AES profiles of elements in the surface layer of Ti/Cu samples after CPF treatment at Q=57 J/cm^2 (a) and Q=74 J/cm^2 (b).

Fig. 5. XRD patterns of Ti/Cu system samples before and after CPF treatment. The angle positions of Cu standard diffraction lines (card file # 04-0836) and α-Ti standard diffraction lines (card file # 44-1294) are indicated by dotted lines.

Fig. 6 XRD patterns (2Θ=71-92^o) of Ti/Cu system samples before and after CPF treatment.

Fig 7. Dependence of the Cu`(Ti) lattice parameter (derived from deconvolution of Cu + Cu`(Ti) (311) diffraction lines) for Cu/Ti system samples treated by CPF on the density of energy absorbed by the surface. The lattice parameter of Cu standard is equal to 0,3615 nm (card file # 04-0836).

Fig. 8. Microhardness of Cu sample and Ti/Cu system samples after CPF treatment.

Fig. 9. Friction coefficient dependence on the indenter sliding distance of Cu sample and Ti/Cu system samples after CPF treatment.

Fig. 10. Wear tracks (optical microscopy) in Cu sample (a) and Ti/Cu system sample after CPF treatment at Q=74 J/cm^2 (b).

Fig. 1

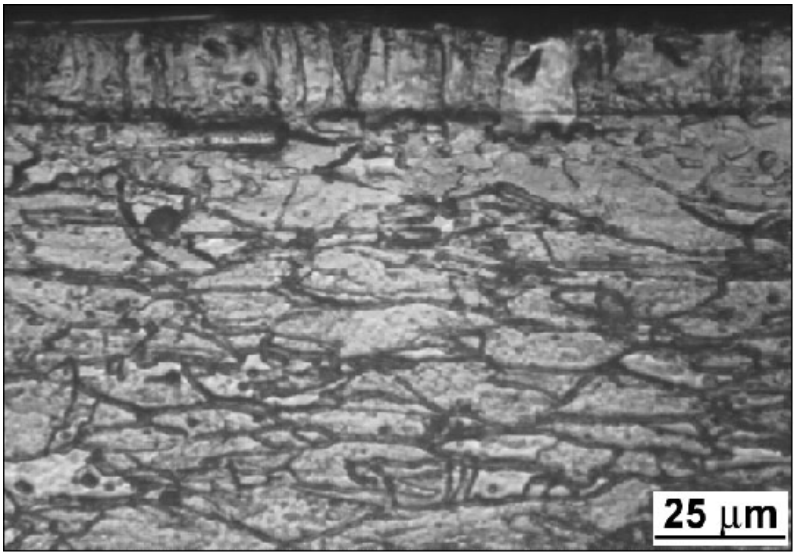

Fig. 2

a)

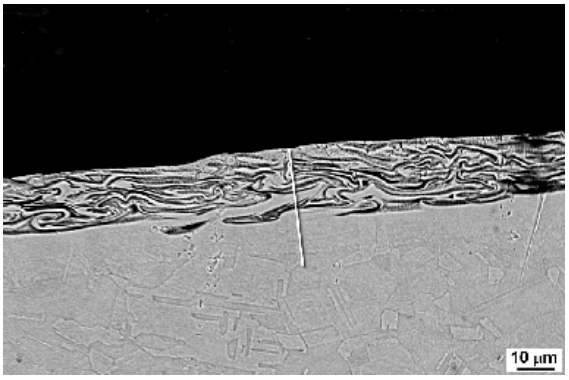
10 µm

b)

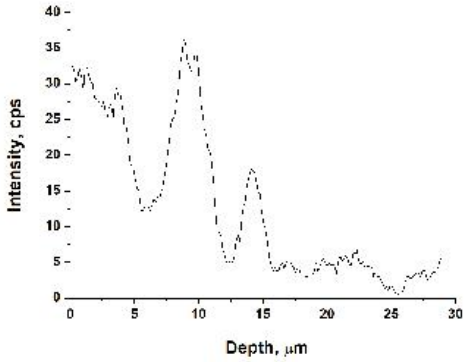
Intensity, cps
Depth, µm
0
5
10
15
20
25
30
35
40

c)

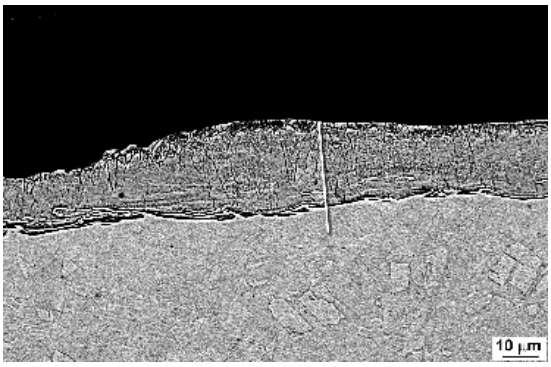
10 µm

d)

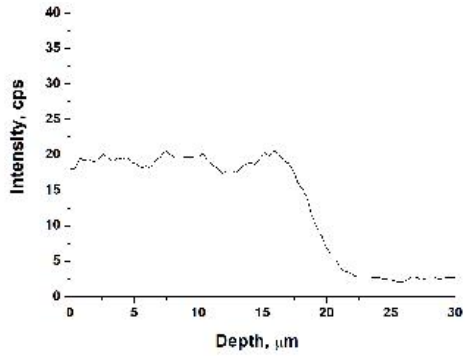
Intensity, cps
Depth, µm
0
5
10
15
20
25
30
35
40

Fig. 3

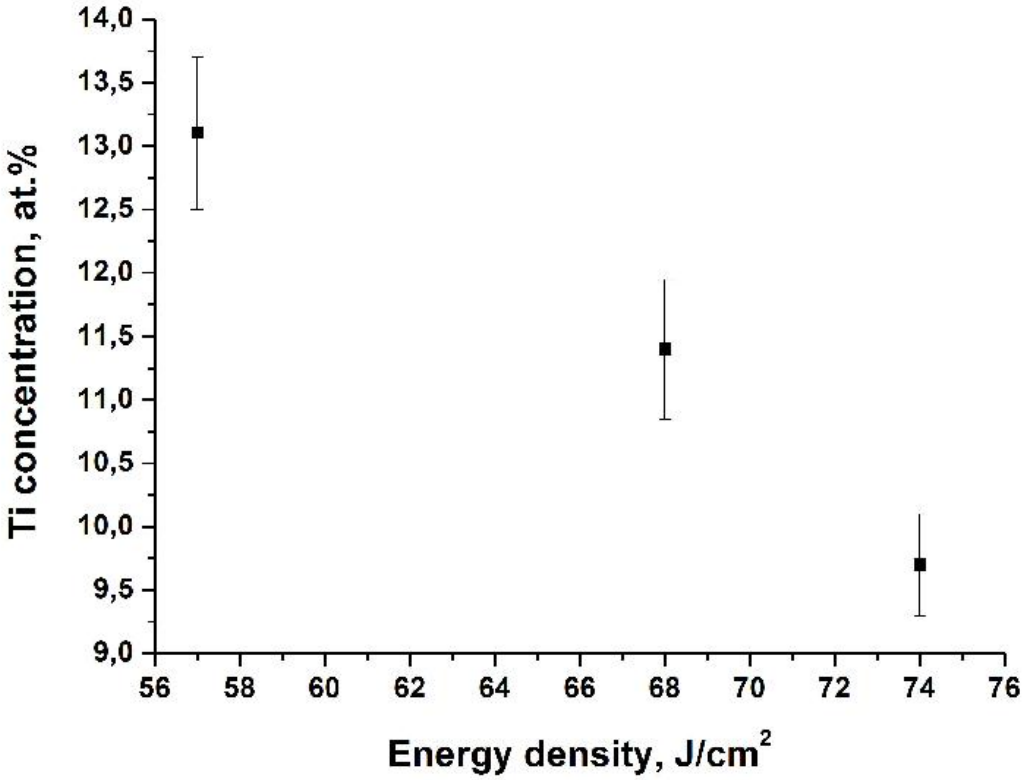
Ti concentration, at.%
14,0
13,5
13,0
12,5
12,0
11,5
11,0
10,5
10,0
9,5
9,0
56
58
60
62
64
66
68
70
72
74
76
Energy density, J/cm2

Fig. 4

a)

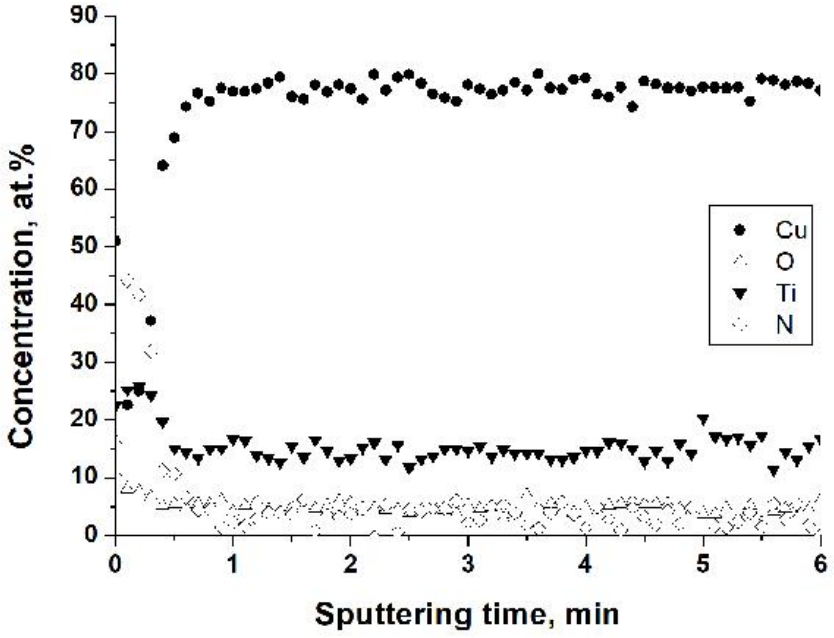
Concentration, at.%
Sputtering time, min
Cu
O
Ti
N

b)

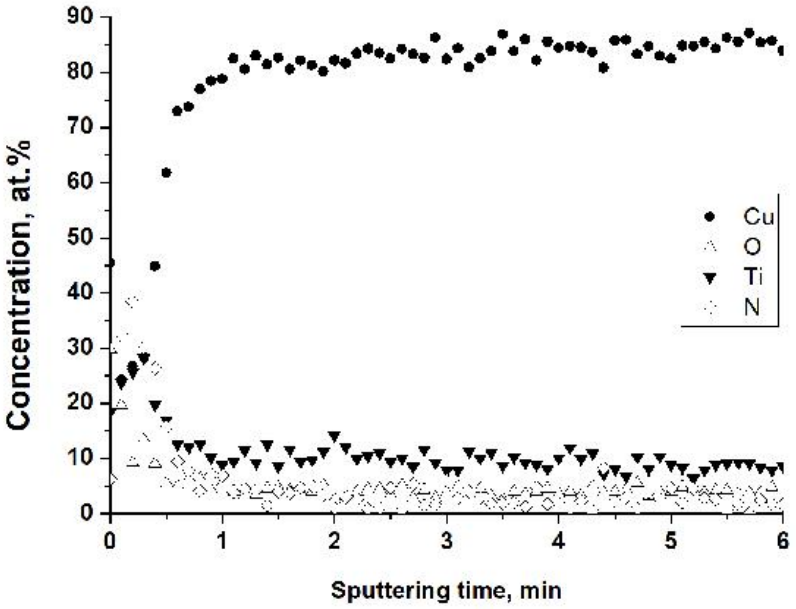
Concentration, at.%
Sputtering time, min
Cu
O
Ti
N

Fig. 5

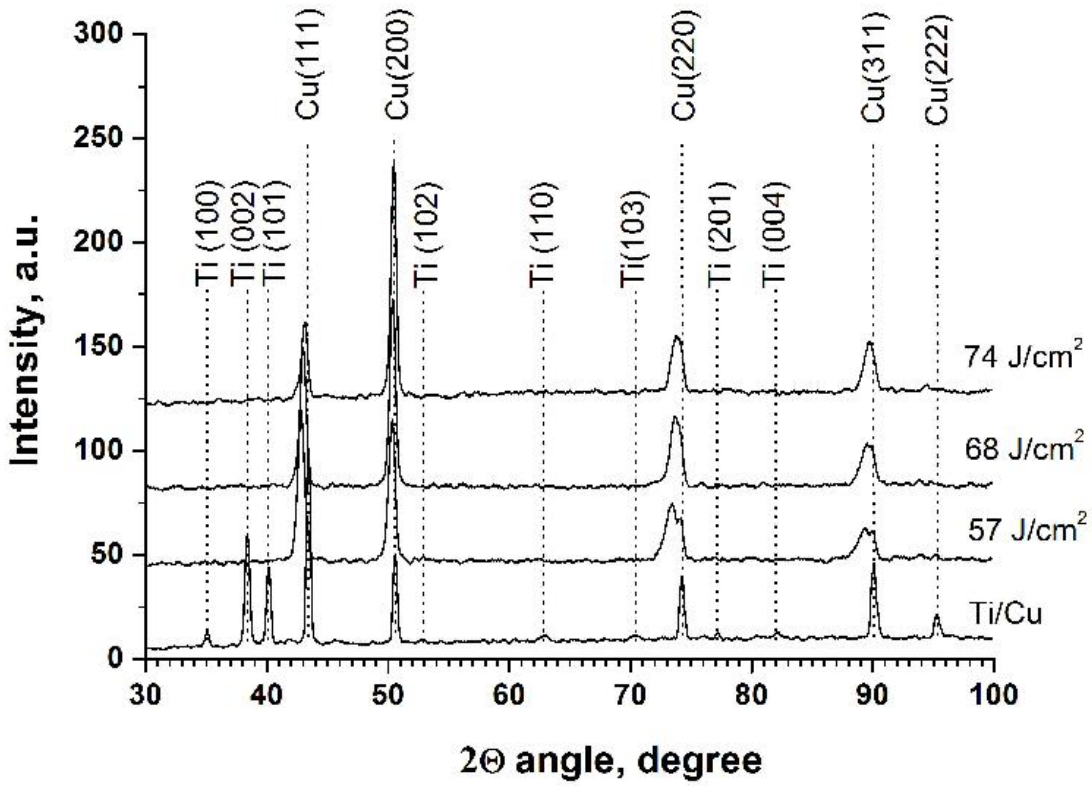
Intensity, a.u.
2Θ angle, degree
Ti (100)
Ti (002)
Ti (101)
Cu(111)
Cu(200)
Ti (102)
Ti (110)
Ti(103)
Cu(220)
Ti (201)
Ti (004)
Cu(311)
Cu(222)
74 J/cm2
68 J/cm2
57 J/cm2
Ti/Cu

Fig. 6

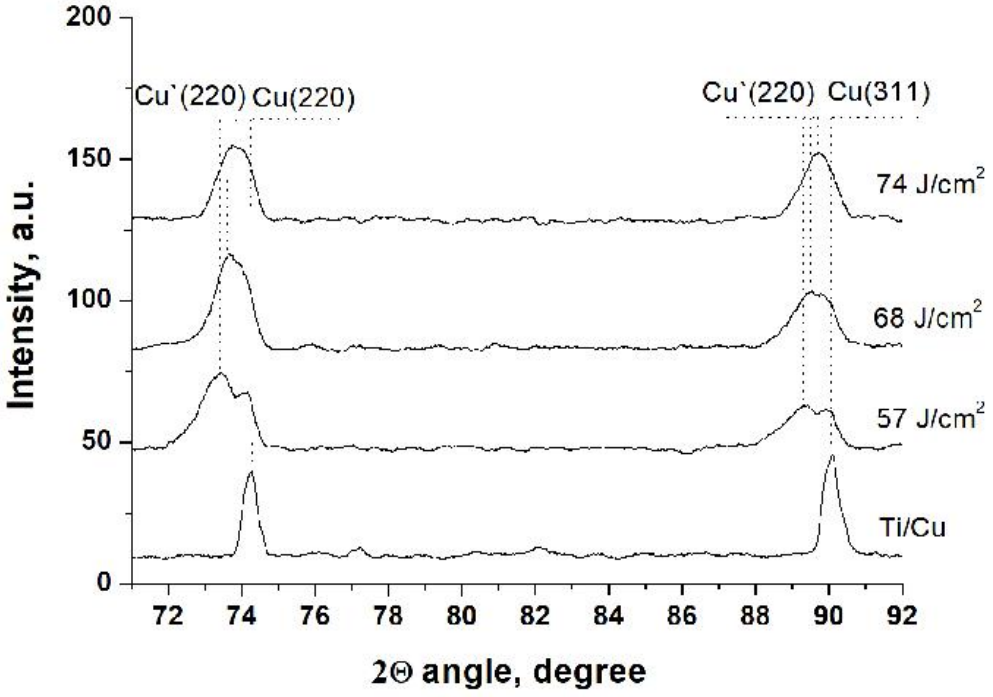
Cu`(220)
Cu(220)
Cu`(220)
Cu(311)
74 J/cm2
68 J/cm2
57 J/cm2
Ti/Cu
Intensity, a.u.
2Θ angle, degree
0
50
100
150
200
72
74
76
78
80
82
84
86
88
90
92

Fig. 7

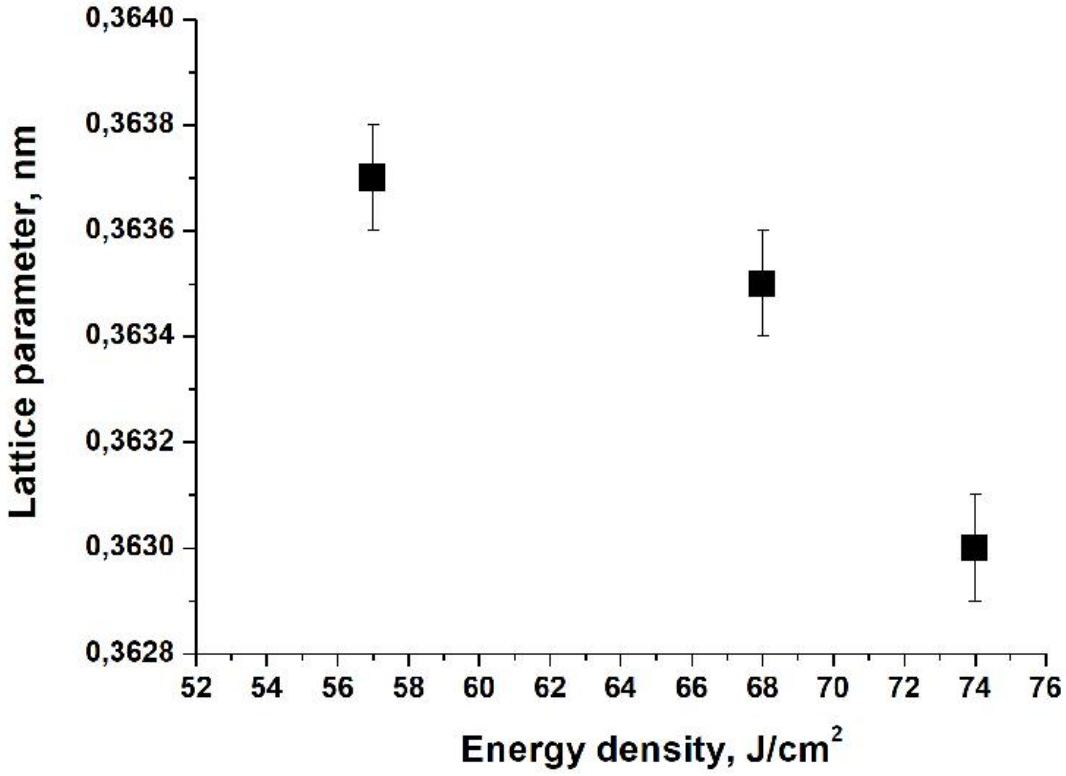
Lattice parameter, nm
0,3640
0,3638
0,3636
0,3634
0,3632
0,3630
0,3628
52
54
56
58
60
62
64
66
68
70
72
74
76
Energy density, J/cm2

Fig. 8

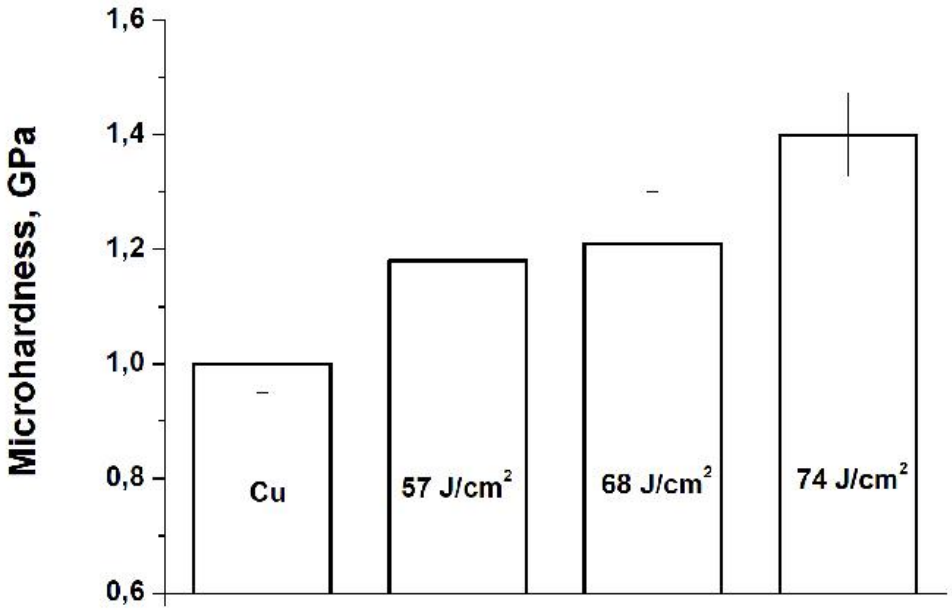

Fig. 9

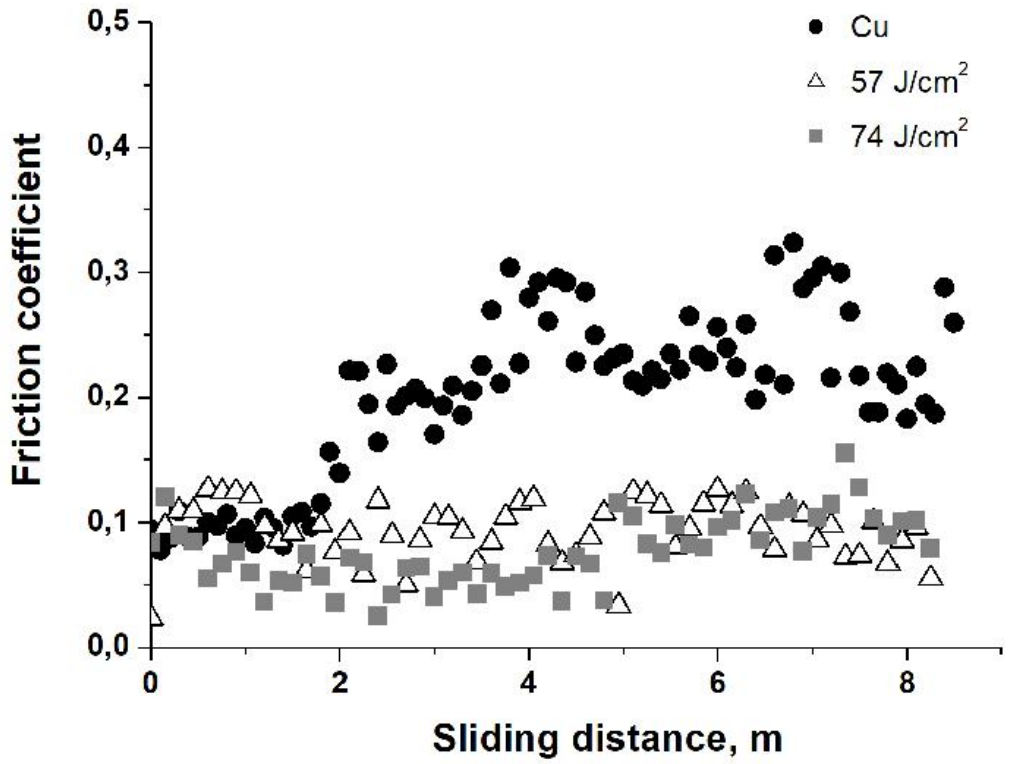
Friction coefficient
0,0
0,1
0,2
0,3
0,4
0,5
0
2
4
6
8
Sliding distance, m
Cu
57 J/cm2
74 J/cm2

Fig. 10

a)

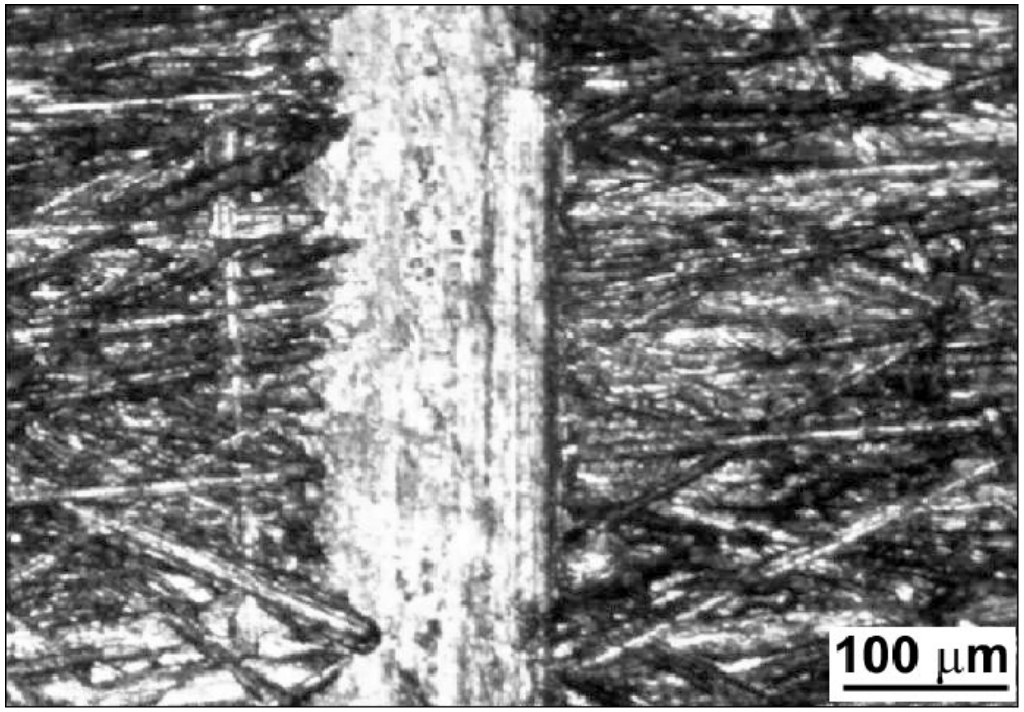

b)